ACS SENSORS

pubs.acs.org/acssensors Article

Aptagel Plasmonic Fiber Optic Biosensor for *In Vivo* Continuous Drug Monitoring

Pragnya Satapathy,[§] Soohyun Park,[§] Anil Pal, Catia Santa, Eliza Koros, Judith Schweimer, Roger Hasler, Jakub Dostalek, Heather Clark, Roberto Arban, Bastian Hengerer, and Khulan Sergelen*

Cite This: *ACS Sens.* 2026, 11, 5858−5868 Read Online

ACCESS | Metrics & More | Article Recommendations | Supporting Information

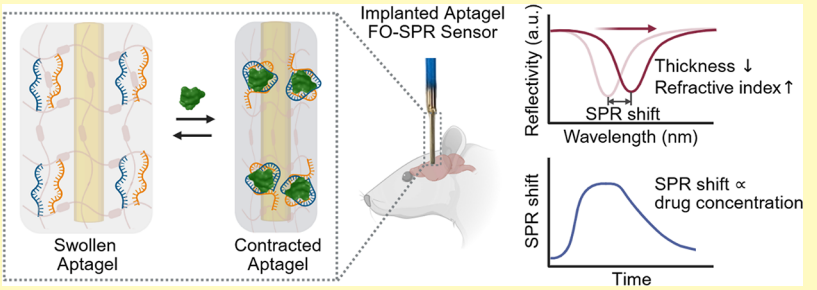

ABSTRACT: Continuous monitoring of drug dynamics directly in living tissue remains a major challenge, notably in the brain, where the blood−brain barrier creates distinct microenvironments. Here, we report an implantable fiber optic surface plasmon resonance (FO-SPR) biosensor coated with aptagel, a split-aptamer-crosslinked hydrogel, for continuous monitoring of a small-molecule drug, vancomycin. The aptagel undergoes analyte-induced volumetric and refractive index changes, providing a self-contained means for reversible, label-free optical detection via shifts in the SPR wavelength (λ_{SPR}) while ensuring sensor stability in complex physiological matrices. The sensing area was miniaturized to 3 mm^2 (3 mm length, 300 μm diameter) for cortical implantation while maintaining sensitivity of >2000 nm/RIU. The sensor performed consistently *in vitro* across diverse biological media, including blood serum, with detection limits of 1.7−2.5 μM. Upon implantation into the rat cortex, time-resolved λ_{SPR} signals were recorded over several hours after intravenous vancomycin administration, representing to our knowledge the first demonstration of plasmonic fiber-based monitoring of a small-molecule drug directly in brain tissue. Baseline-corrected shifts ($\Delta\lambda_{SPR}$) captured *in vivo* drug dynamics, with a consistent absorption phase but with inter-animal variability in peak amplitude and clearance kinetics. This work establishes a proof-of-concept platform for continuous optical monitoring in deep tissue and highlights the potential of FO-SPR sensing for *in vivo* pharmacokinetic applications.

KEYWORDS: *plasmonic fiber optic, aptamer, hydrogel, in vivo, precision medicine*

Continuous and direct monitoring of small molecules, including drugs, metabolites, hormones, and other biomolecular biomarkers within living tissue, represents a significant challenge. Particularly in the brain, the blood−brain barrier (BBB) restricts drug entry and creates distinct pharmacokinetic microenvironments that blood sampling cannot reliably predict.[1,2] Within the brain, regional variations in BBB permeability, cell types, and metabolic enzyme activity significantly affect drug distribution,[3] highlighting why local tissue monitoring is important. While immunoassays[4−6] and liquid chromatography-mass spectrometry[7−9] serve as gold standard methods, these only provide data at discrete times, limiting the ability to capture continuous changes in living subjects. Direct access to time-resolved molecular concentrations in target tissues would enable deeper understanding of drug distribution and local responses under physiological conditions.[10,11] In this context, implantable sensing technologies offer a promising approach for probing tissue-level pharmacokinetic and pharmacodynamic relationships with high spatiotemporal resolution.[10]

Various sensing platforms have been explored for continuous *in vivo* monitoring. Early approaches utilizing simple fluorescent dye encapsulation with labeled receptors[12−14] and colorimetric detection relying on plasmonic nanoparticles functionalized with affinity-based receptors[15,16] lack self-confinement, are prone to signal loss, and require complex detection or imaging setups, limiting their suitability for long-term *in vivo* applications.[17,18] Electrochemical aptamer-based (EAB) sensors have

Received: February 13, 2026
Revised: June 8, 2026
Accepted: June 15, 2026
Published: June 23, 2026

https://doi.org/10.1021/acssensors.6c00681
ACS Sens. 2026, 11, 5858−5868

been successful in *in vivo* monitoring of drugs or metabolites at sub-minute temporal resolution through analyte-induced aptamer conformational changes that modulate electron transfer from redox labels, with implantation studies in rodent brains and veins, enabling continuous pharmacokinetic measurements.[19−21] Building on this, recent reports have utilized microneedle arrays with EAB sensors to enable continuous monitoring of analytes in interstitial fluid, highlighting strong potential for clinical translation.[22] Although microneedle-based platforms are well suited for peripheral tissues as wearable sensors, their extension to direct measurements within deep tissue such as the brain remains challenging.

In parallel, implantable optical sensors, mainly fiber optic (FO)-based biosensors, have been widely explored for *in vivo* molecular detection, leveraging optical transduction mechanisms that integrate molecular recognition and signal generation within a single platform.[23−31] Such systems inherently eliminate the need for reference electrodes and are largely immune to electromagnetic interference. By utilizing optical transduction mechanisms such as fluorescence and surface-enhanced Raman scattering (SERS), *in vivo* molecular sensing of proteins such as nitroreductase for tumor or S100β for neuroinflammation has been reported.[32,33] However, many implementations often require exogenous labels and rely on endpoint analysis rather than stable, continuous monitoring of molecules. These considerations underscore the need for sensing architectures that combine molecular specificity with robust, label-free signal transduction for prolonged operation in complex tissue environments, capable of resolving the changing concentrations of various-sized molecules.

Across sensing modalities, hydrogels and polymeric coatings have been extensively employed to improve biocompatibility, reduce biofouling, and extend operational lifetimes of implantable sensors. In particular, protective layers such as agarose,[34] antimicrobial coating,[35] and hydrogels[36,37] have extended sensor lifetimes from hours to days or weeks in various *in vivo* contexts. Motivated by these advances, we recently developed a molecularly responsive hydrogel matrix containing aptamers (aptagel) that integrates molecular recognition with an SPR readout for direct, continuous monitoring of small molecules.[38] The aptagel architecture embeds abundant receptors within a 3D matrix rather than directly on the sensing surface; therefore, it enhances stability through ensemble-averaged measurements and protects aptamers from rapid degradation or fouling. Also, aptagel undergoes reversible transduction upon analyte binding, generating measurable refractive index changes, and exhibits markedly improved stability in biological fluids such as serum from several days to weeks.

Here, we report an advanced aptagel-coated FO-SPR sensor designed for stable *in vivo* biosensing. Our work represents the first demonstration of a direct, plasmonic fiber sensor capable of continuous detection of the small-molecule drug, vancomycin, in the brain of anesthetized rats over a 5 h period. To enable cortical implantation in rats, we minimized the sensing area to 3 mm^2 (3 mm length, 300 μm fiber core), while preserving the sensitivity of >2000 nm/RIU after aptagel incorporation, comparable to larger FO-SPR probes.[29,31,39,40] Our system operates via wavelength-modulated SPR in a compact lab-on-fiber platform. The sensor performance was validated *in vitro* in complex biological fluids, including diluted blood plasma and whole serum, demonstrating reliable detection at 1−2 μM vancomycin concentrations before *in vivo* application. Overall, the design of this self-contained, biocompatible optical probe establishes a platform for minimally invasive, tissue-level monitoring, supporting future applications in *in vivo* therapeutic drug sensing.

■ RESULTS AND DISCUSSION

Implantable Aptagel FO-SPR Sensor Design

Our proposed sensor architecture, termed aptagel, leverages split-aptamer pairs that are strategically divided into two segments that reconstitute their binding function only in the presence of target molecule, as previously validated and further illustrated in Figure S1.[41,42] The split design was selected to minimize background hybridization while enabling target-induced assembly through cooperative binding. As reported previously, the interaction can be described by a two-step biomolecular interaction model in which the split segments (S1 and S2) exhibit weak intrinsic hybridization affinity in the absence of analyte, whereas binding of vancomycin stabilizes the assembled S1−vancomycin−S2 ternary complex.[42] These split-aptamer pairs are used as structural crosslinkers within an star-shaped eight-arm poly(ethylene glycol)-norbornene (PEG-NB) hydrogel network (Figure 1A).[38] In this configuration, target-induced ternary complex formation triggers contraction of the polymer network leading to decreased swelling and respective increase in refractive index. This mechanism was experimentally validated in our previous work using angular SPR measurements, where shifts in aptagel waveguide modes (probing depths of ∼10 μm) directly captured reversible hydrogel contraction upon analyte binding and reswelling upon the analyte dissociation (Figure S2).[38]

Unlike the conventional approach to post-functionalize aptamers by tethering them within the hydrogel network, the aptagel incorporates dithiolated split-aptamer pairs as integral structural components via thiol-norbornene click chemistry, achieving exceptionally high aptamer densities (up to 30% of total crosslinking moieties, 3 mM in final concentration), while maintaining the network homogeneity.[38] Upon target binding, the local refractive index of aptagel ($\Delta n_{aptagel}$) changes, generating a corresponding shift in the SPR resonance wavelength ($\Delta\lambda_{SPR}$) that is monitored in real time. The magnitude of $\Delta\lambda_{SPR}$ correlates directly with $\Delta n_{aptagel}$ near the gold surface, with analyte binding producing a characteristic red shift.

In this study, we translated this planar surface-optimized aptagel platform to a miniaturized FO-SPR format for implantation into rat brain (Figure 1B). The *in vivo* measurement setup comprises a compact optical configuration designed for continuous molecular monitoring in brain tissue. The FO probe connects to a broad-spectrum light source and spectrometer via a Y-coupler, enabling real-time signal acquisition during *in vivo* PK measurement. The aptagel matrix serves dual functions: providing an antifouling interface that could potentially minimize tissue inflammatory responses while facilitating selective analyte recognition through self-contained receptors.[38] The 3D hydrogel architecture enhances optical signal transduction of refractive index changes compared to its monolayer counterpart without compromising temporal resolution (affected by analyte diffusion) that is essential for the rapid association and dissociation kinetics of aptamer−drug complexes enabling continuous tracking of drug concentration. Additionally, the aptagel coating aims to improve sensor stability by preserving aptamer

https://doi.org/10.1021/acssensors.6c00681
ACS Sens. 2026, 11, 5858−5868

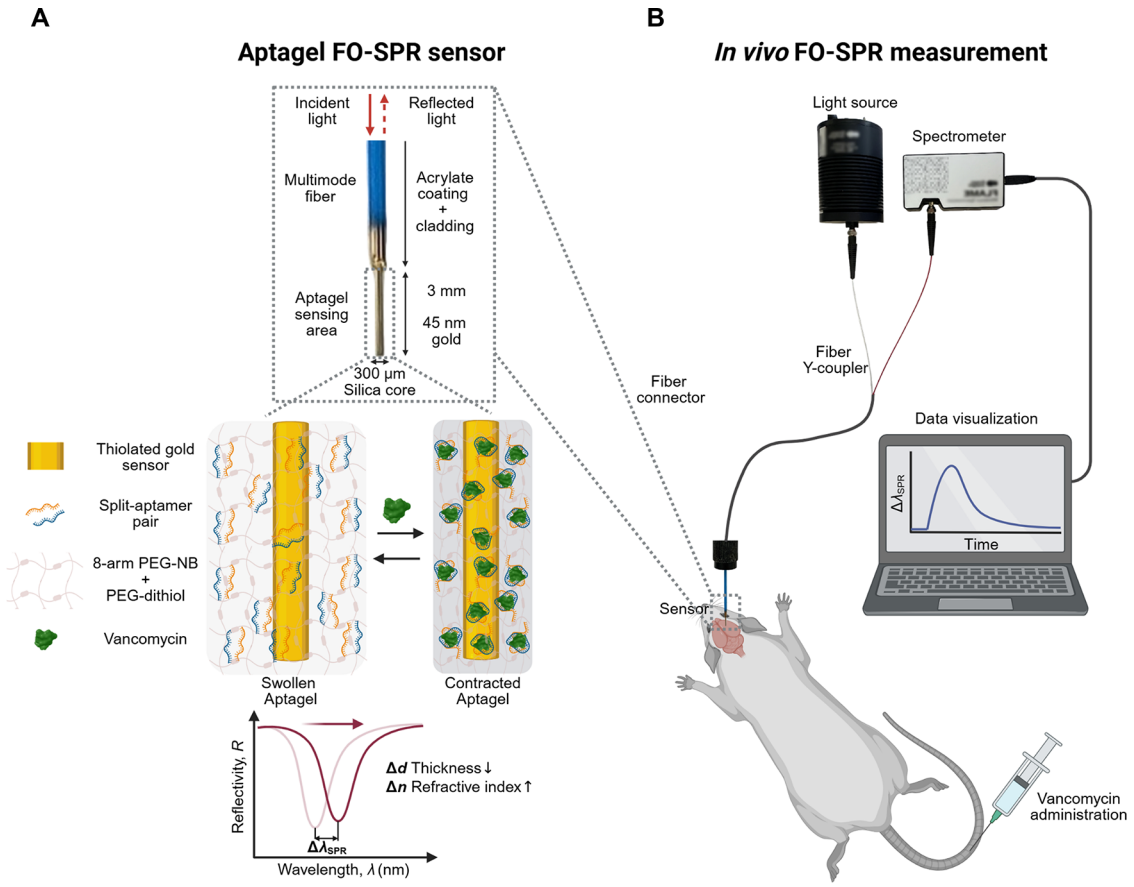

Figure 1. Schematic of an aptagel-coated implantable FO-SPR sensor for *in vivo* drug monitoring in the rodent brain. (A) Sensor architecture comprises a 300 µm diameter silica core, a 45 nm thick gold layer, and aptagel coating with a 3 mm sensing length. Incident white light propagating through the optical fiber core generates SPR at the gold-dielectric interface containing the aptagel film. Vancomycin binding to split-aptamer pairs forms ternary complexes within the aptagel matrix, resulting in hydrogel contraction that decreases the film thickness (d) while increasing the local refractive index ($n_{aptagel}$), manifesting as an SPR wavelength (λ_{SPR}) red shift. (B) The optical setup consists of a light source and a spectrometer connected via the Y-coupler to the FO-SPR sensor. The hydrogel matrix provides biocompatible, antifouling properties while transducing reversible binding events into measurable optical signals for continuous PK monitoring.

functionality and shielding the sensing interface from protein adsorption.

Aptagel FO-SPR Sensor Characterization

Electrochemical sensors designed for minimally invasive implantation and monitoring of different brain regions in rodents demonstrated optimal dimensions of ≤100 µm in diameter with sensing lengths ranging from 3 to 5 mm.[43,44] In contrast, FO-based sensors often require larger dimensions to assure adequate strength and stability of optical signal transmitted via the fiber core. While longer fiber probes provide enhanced sensitivity due to increased interaction area with the surrounding medium,[45] smaller diameters in multimode fibers decrease the number of guided optical modes, ultimately decreasing sensitivity.[29] Previously reported FO-SPR sensors have demonstrated diameters of ≥400 µm and lengths of ≥5 mm to achieve bulk sensitivity values of ∼2000−3000 nm/RIU.[29,39,40]

To enable implantation in rat brain tissue, we reduced the sensor probe dimensions to 3 mm in length and 300 µm in diameter, representing a 2.2-fold reduction in sensing area compared to previously reported multimode FO-SPR sensors. A schematic representation of the FO-SPR sensor configuration for continuous *in vitro* monitoring is presented in Figure 2A. The FO-SPR probe was positioned in a microfluidic chamber with a controlled flow and temperature to simulate physiological conditions and minimize the effect of diffusion-limited mass transfer that slows down sensor response kinetics. This controlled environment maintained consistent analyte delivery at 37 °C, enabling accurate sensor validation prior to *in vivo* deployment.

Optical characterization of the aptagel FO-SPR sensors revealed significant changes in spectra compared to bare gold probes (Figure 2B). Aptagel integration alters the dielectric properties surrounding the FO-SPR probe, where the higher refractive index aptagel ($n_{aptagel}$ ∼1.348) increases the effective refractive index of the medium and introduces surface plasmon damping.[40,46] These optical changes affect reflectivity spectra with encoded SPR. The bare FO-SPR probe exhibited a λ_{SPR} at ∼630 nm, which underwent a red shift of ∼30 nm upon aptagel incorporation due to the increased refractive index. Aptagel functionalization also reduced the overall reflected intensity and broadened the SPR spectral linewidth, consistent with plasmon damping effects.

We then determined sensitivity values by measuring the $\Delta\lambda_{SPR}$ responses to Δn using a series of sucrose solutions,

https://doi.org/10.1021/acssensors.6c00681
ACS Sens. 2026, 11, 5858−5868

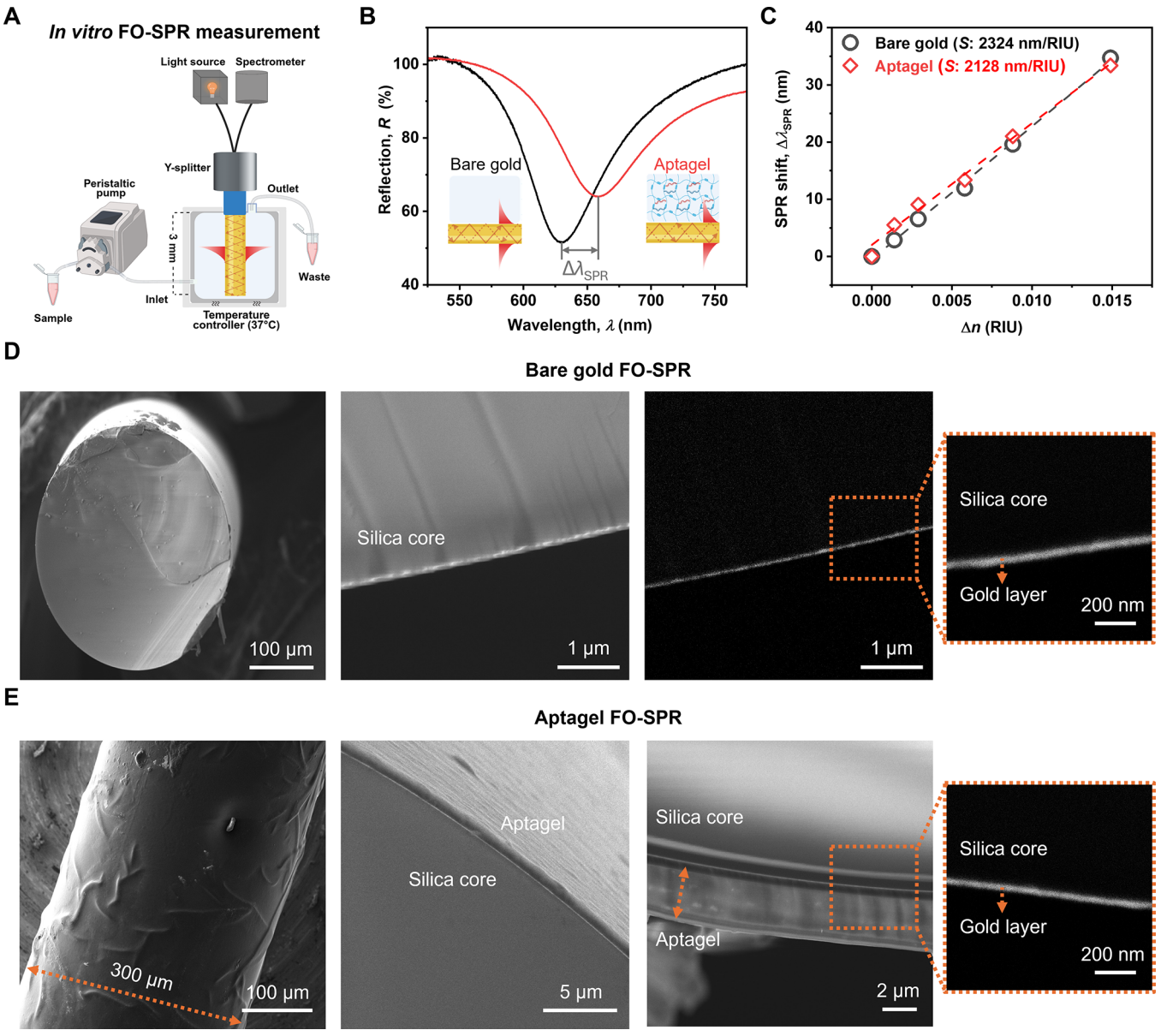

Figure 2. Aptagel FO-SPR sensor characterization. (A) Schematic of the *in vitro* measurement setup. Temperature-controlled flow cell maintains 37 °C with continuous fluid exchange. (B) Reflection spectra of bare gold and aptagel FO-SPR sensors showing aptagel-induced $\Delta\lambda_{SPR}$. (C) Bulk sensitivity (S) determination: λ_{SPR} vs refractive index change (Δn) using graded sucrose solutions. Linear fits yield S values for bare gold and aptagel sensors. (D) Cross-sectional SEM images of bare gold FO. The silica core is clearly resolved, and a thin gold layer is visible at the surface. The third image and the higher-magnification view (right) were acquired in backscattered electron (BSE) mode to highlight the gold coating with enhanced compositional contrast relative to the silica. (E) SEM images showing surface and the cross-sectional views of aptagel FO-SPR. The aptagel layer is observed on top of the gold-coated silica core. The corresponding high-magnification BSE image (right) reveals the underlying gold layer, confirming the multilayer structure.

which provide linearly varying refractive indices suitable for bulk sensitivity (S) characterization.[47] Linear regression analysis yielded S values of 2324 and 2128 nm/RIU for bare gold and aptagel FO-SPR sensors, respectively (Figure 2C). While aptagel functionalization resulted in spectral broadening and a modest 10% reduction in S, these values remain comparable to previously reported FO-SPR sensors with larger sensing areas.[29,39,40] From our experimental S values, we calculated the $n_{aptagel}$ by determining the ratio of $\Delta\lambda_{SPR}$ to Δn and then adding the baseline refractive index of water. The calculated $n_{aptagel}$ value was averaged across three independent aptagel FO-SPR sensors as 1.3476 ± 0.0020 RIU, demonstrating an excellent agreement with values previously obtained using angular SPR configurations.[38] Nevertheless, the modest reduction in S observed with aptagel-coated sensors can be attributed to the polymer network that occupies a small fraction of sensing volume; however, the highly swollen three-dimensional structure maintains efficient analyte access to the sensing interface.

To validate the fabricated sensor architecture, we examined cross sections of bare gold and aptagel FO-SPR probes using

https://doi.org/10.1021/acssensors.6c00681
ACS Sens. 2026, 11, 5858−5868

a scanning electron microscope (SEM), which reveals the multilayer structure of our sensor. SEM analysis confirmed a sputtered gold layer thickness of ∼45 nm on the silica core (Figure 2D), which is particularly visible in backscattered electron (BSE) mode, enabling enhanced compositional contrast of the gold coating (the third image and magnified view on the right). The dehydrated aptagel coating appeared as characteristic surface ripples in the dried state, with measured dry thickness ranging from 1 to 3 μm (Figure 2E). In the high-contrast BSE image (the last image), the distinct gold layer is clearly visible, further confirming the multilayer structure of the aptagel FO-SPR sensor. Based on the swelling ratio previously reported,[38] we estimated the hydrated gel layer thickness to range from 9 to 27 μm under aqueous conditions. Notably, this swollen gel thickness significantly exceeds the effective probing depth of the evanescent surface plasmon field (∼200 nm), ensuring complete coverage of the sensing region while maintaining efficient analyte diffusion through the porous hydrogel matrix.

In Vitro Aptagel FO-SPR Sensing Performance

Following fabrication and optical and electron microscopy characterization, we deployed the aptagel FO-SPR sensor for *in vitro* vancomycin monitoring using a continuous flow system with controlled fluidic exchange. We performed sensing measurements by first equilibrating the sensor in assay buffer, PBS supplemented with 2 mM $MgCl_2$ to promote folding and structural stability of aptamers during binding assays.[48] Then, the sensor was exposed to decreasing vancomycin concentrations ranging from 500 to 0.5 μM, with buffer wash steps between each concentration to test reversibility (Figure 3A). The aptagel FO-SPR sensors demonstrated excellent reversibility and stable baseline recovery, confirming robust sensor performance across multiple analyte exposure cycles.

Dose−response analysis revealed two distinct SPR shift regimes with apparently different sensitivities (Figure 3B). At concentrations below ∼60 μM, the sensors exhibited a linear relationship between $\Delta\lambda_{SPR}$ and log(c), achieving a limit of detection (LOD) of 2.1 μM for vancomycin in assay buffer. Notably, for concentrations above ∼60 μM, the sensor response transitioned to a different, non-linear dependence on log(c) with enhanced sensitivity but higher measurement variability. This amplification arises from mechanical contraction of the hydrogel matrix driven by a ternary complex formation between crosslinked split-aptamer pairs and vancomycin, enhancing signal output compared to classical antigen-based binding. This biphasic response profile demonstrates the enhanced sensitivity of split-aptamer pairs embedded within the hydrogel matrix, as previously reported.[38] While increased variability due to the transition between two distinct response regimes occurs at higher analyte concentrations far from the determined LOD, the accessible dynamic range aligns well with clinically relevant

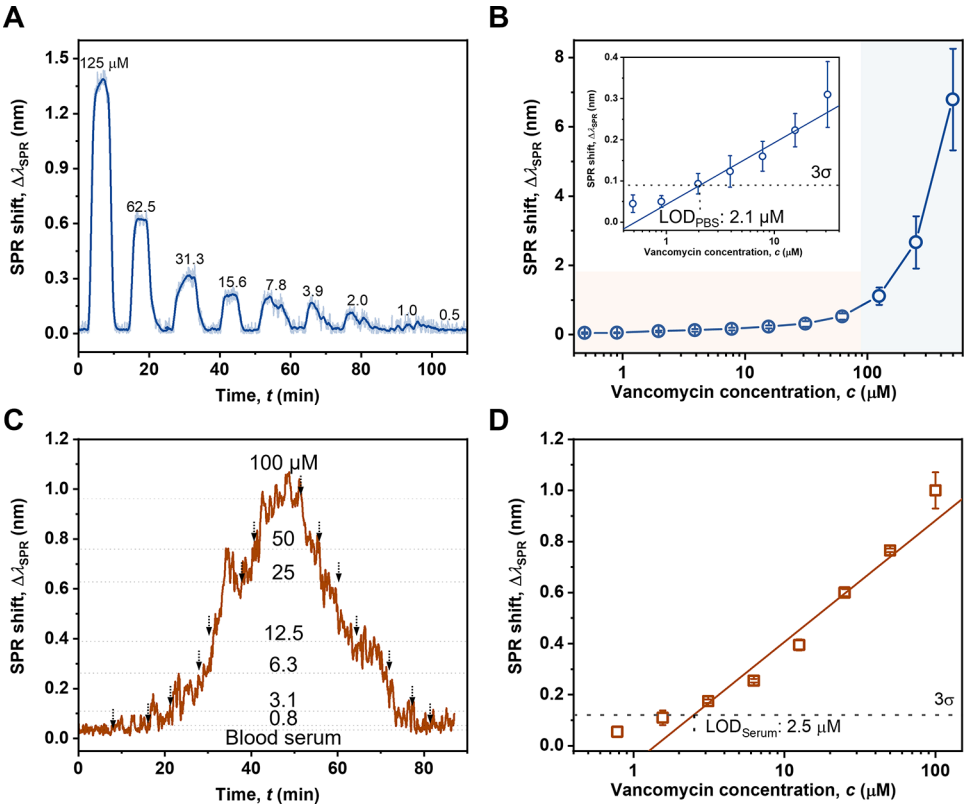

Figure 3. *In vitro* characterization of aptagel FO-SPR sensor response to vancomycin. (A) Continuous vancomycin monitoring in assay buffer demonstrating reversible responses across multiple concentrations (125 to 0.5 μM). Shaded areas represent standard deviation obtained from $n = 3$ measurements. (B) Dose−response curve showing biphasic behavior with distinct low- and high-concentration regimes (indicated by orange and blue shadings, respectively). Inset: linear calibration curve for the low concentration range (Pearson's $R^2 = 0.98$, $LOD_{PBS} = 2.1$ μM). (C) Continuous monitoring in blood serum with increasing and decreasing vancomycin concentrations. Arrows indicate injection concentrations. Rapid dissociation kinetics enable sensor recovery within physiologically relevant timeframes. (D) Dose−response curve in serum (Pearson's $R^2 = 0.98$, $LOD_{Serum} = 2.5$ μM). All error bars represent standard deviations ($n = 3$ sensors).

https://doi.org/10.1021/acssensors.6c00681
ACS Sens. 2026, 11, 5858−5868

vancomycin concentrations, which typically range from 6 to 30 μM in blood and brain tissue of rodents.[20,49,50]

To establish sensor performance under physiologically relevant conditions, we evaluated continuous vancomycin monitoring in complex biological fluids prior to *in vivo* deployment. We tested our sensors in 20% diluted human blood plasma and undiluted horse serum, which contain rich spectrum of proteins (albumin ∼60%, globulins ∼30%, fibrinogen ∼4%, and other regulatory proteins ∼1%),[51,52] providing assessment of the antifouling properties of aptagel. Non-specific interactions in complex biological matrices can significantly compromise sensing performance, particularly for SPR-based sensors that respond to surface mass density variations at the gold-solution interface.[53]

Continuous vancomycin monitoring in undiluted horse serum demonstrated robust sensor performance with clear concentration-dependent responses (Figure 3C). The sensorgram shows a gradually increasing response to sequential vancomycin injections from 0.8 to 100 μM, with each concentration producing distinct SPR shifts followed by reproducible signal recovery during the decreasing concentration phase. The corresponding calibration curve (Figure 3D) exhibits linearity across the low concentration range of log(c) with an LOD of 2.5 μM. Similarly, measurements in diluted human plasma (20%, Figure S1) achieved an LOD of 1.7 μM, demonstrating preserved sensor performance compared to the assay buffer (LOD: 2.1 μM).

These results confirm that the aptagel coating effectively maintains sensor sensitivity and selectivity in complex protein-rich biological matrices, with minimal impact on detection limits across different physiological media. Next, we also evaluated the specificity of the aptagel FO-SPR sensors against relevant antibiotics, including bacitracin, rifampicin, and ampicillin, with concentrations adjusted to match the refractive index of 30 μM vancomycin, confirming the selectivity by showing negligible responses from all non-target drugs (Figure S2).

In Vivo Vancomycin Monitoring Using Aptagel FO-SPR

Following validation in complex biological fluids, we deployed the aptagel FO-SPR sensor for continuous plasmonic fiber-based drug monitoring in live rodent brain tissue. Sensors were stereotactically implanted into the left cortex via craniotomy, and λ_{SPR} signals were continuously recorded (∼3 s resolution) in anesthetized rats. A saline control experiment was conducted to characterize baseline drift over 4 h (raw data in Figure S5A). Injection-related signal was not observed, and the baseline gradually approached a stable plateau after ∼3 h, which is significantly longer than the 40−60 min stabilization typically observed *in vitro*. This prolonged equilibration is attributed to dry-state implantation of the sensor, requiring *in situ* hydrogel reswelling within brain tissue. The baseline was well described by a two-phase exponential decay ($R^2 = 0.996$), which was subsequently used to model and correct the baseline in drug response analyses. Due to experimental time constraints (6 h), a shorter stabilization period (1−2 h) was applied prior to intravenous tail vein vancomycin administration.

A total of four rats were administered with 75 mg/kg vancomycin, a dose that exceeds standard clinical ranges but is consistent with rodent pharmacokinetic studies of brain extracellular fluid (ECF) monitoring given the limited BBB permeability of vancomycin.[20,54,55] Raw λ_{SPR} signals and corresponding baseline fits (applied from implantation to pre-injection) are presented in Figure 4 with full time-scale data provided in

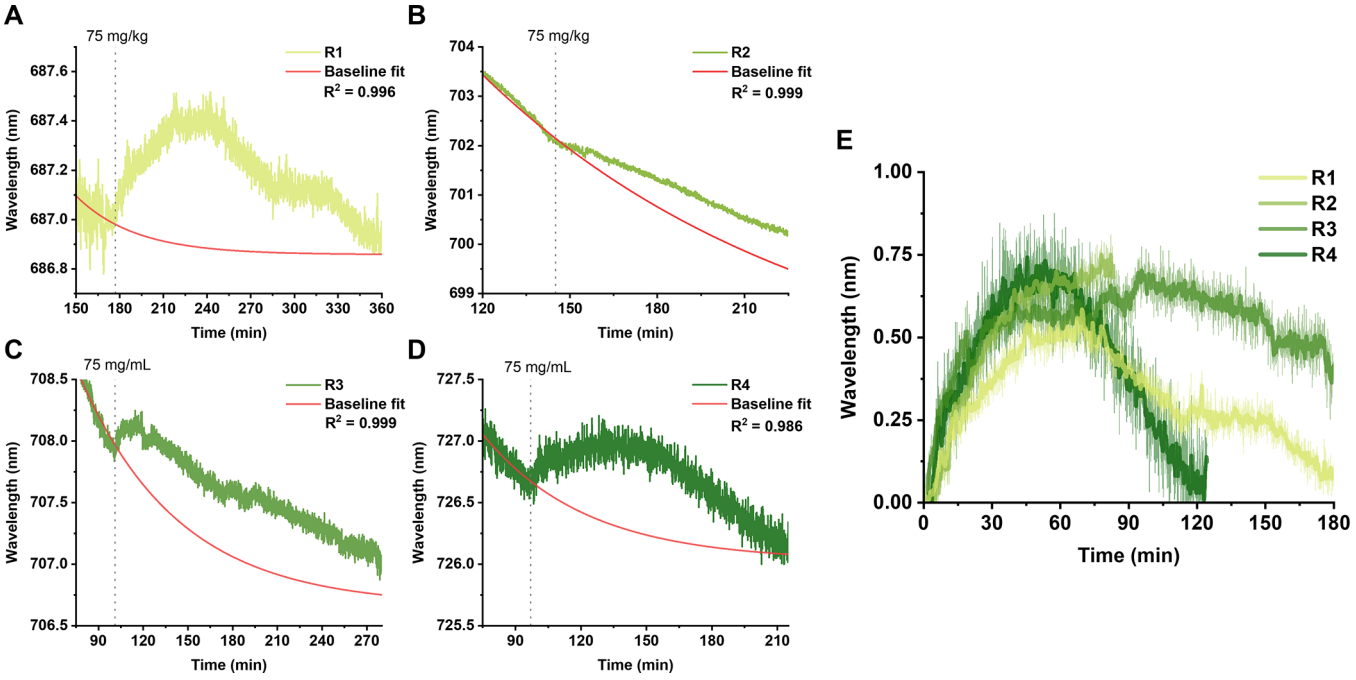

Figure 4. *In vivo* monitoring of vancomycin in rat brain using the aptagel FO-SPR sensor. (A−D) Representative λ_{SPR} responses from four individual rats after implantation in the cortex and intravenous tail vein administration of vancomycin (75 mg/kg). Red curves indicate two-phase exponential fits applied from implantation to pre-injection for baseline fitting. Full time-scale data including pre-injection baseline are provided in Figure S5. (E) Baseline-corrected wavelength shifts ($\Delta\lambda_{SPR}$) aligned to the time of injection ($t = 0$) enable comparison of temporal drug response profiles across animals. All traces exhibit an increase following administration, reaching a peak at ∼1 h followed by gradual decay. Data were acquired at ∼3 s intervals in anesthetized rats.

https://doi.org/10.1021/acssensors.6c00681
ACS Sens. 2026, 11, 5858−5868

Figure S5. Across all cases, the baseline exhibits a gradual drift that approaches stability after ∼3 h, with noticeable inter-animal variability in magnitude (black curves). Despite this variability, a clear response associated with drug absorption in brain tissue was evident in all animals. The baseline fitting by the two-phase exponential decay model is presented in red curves ($R^2 > 0.99$).

After baseline correction, $\Delta\lambda_{SPR}$ signals aligned to the injection time (Figure 4E) showed a more comparable response across animals. $\Delta\lambda_{SPR}$ increased after administration, reaching a peak at ∼1 h followed by a gradual decline. While variability in amplitude persists, the overall temporal profiles were reproducible. The average of peak wavelength $\Delta\lambda_{SPR}$ was 0.55 ± 0.05 nm at 1 h, corresponding to vancomycin concentration of ∼20 μM based on our serum calibration. This value is roughly two-fold higher than previously reported brain concentrations based on EAB sensor measurements.[3,20,55] The independent vancomycin concentration measured in plasma samples obtained by mass spectroscopy (MS) at 1 h post-injection yielded 82.7 ± 15.2 μM ($n = 2$), consistent with prior reports at comparable dosing levels.[3] Based on a previous microdialysis report noting that vancomycin penetration into brain ECF is typically ∼5−10% of plasma levels,[56] the present measurements are elevated twofold as well.

There could be several factors for this discrepancy. The FO-SPR probe with a relatively large diameter (∼300 μm) compared to EAB-based sensors (∼50 μm) may induce more pronounced local tissue disruption during implantation causing minor bleeding, which potentially may increase local drug exposure or affect clearance rate. In addition, although the two-phase exponential function provides an effective empirical description for baseline correction, residual uncertainty remains in quantification. Accordingly, $\Delta\lambda_{SPR}$ is interpreted primarily as a measure of relative drug dynamics rather than exact concentration.

Notably, greater variability was observed during the drug elimination, which suggests differences in clearance kinetics across animals. The elimination in blood, unlike brain, is more rapid and consistently resolved, as reported in earlier studies,[54,57] reflecting systemic clearance. Among brain measurements under comparable dosing conditions, differing profile characteristics were reported depending on the animal model. Mouse cortex measurements using EAB sensors showed plateau-like concentration profiles with no clearly resolved elimination phase over the experimental timeframe,[3,20] whereas rat studies using simultaneous vein/brain measurements or direct tissue analysis reported first-order elimination phases.[55] Our rat cortical measurements are more consistent with the latter observations, exhibiting gradual elimination over several hours following tail vein intravenous administration. While these observations are broadly consistent with those previously reported in different animal models, experimental factors including the brain compartment region, local diffusion/perfusion conditions, sensor sensitivity, and calibration approach may also contribute to differences in the observed pharmacokinetic profiles.

Although precise pharmacokinetic parameters cannot yet be reliably extracted due to baseline correction and calibration constraints, the FO-SPR platform could resolve relative differences in *in vivo* drug dynamics. This work establishes a proof-of-concept demonstration of FO-SPR-based monitoring of a small-molecule drug directly in brain tissue, enabling real-time observation of drug dynamics and inter-individual variability in clearance. Future advances, including individual sensor calibration and extended pre-measurement stabilization (*e.g.*, chronic implantation), are expected to further improve quantitative accuracy.

■ CONCLUSIONS

We have demonstrated the first implantable plasmonic fiber optic sensor functionalized with a molecularly responsive hydrogel matrix (aptagel) for continuous monitoring of vancomycin directly within living brain tissue. By integrating aptagel with miniaturized FO-SPR probes, we achieved label-free optical detection of vancomycin in rat brain ECF over 6 h with ∼3 s temporal resolution. The compact dimensions of our sensor (3 mm^2 sensing area) enabled cortical implantation while maintaining high sensitivity (∼2000 nm/RIU). While baseline drift and calibration constraints currently limit quantification, the sensor could reproducibly resolve relative drug dynamics and reveals inter-individual variability in clearance kinetics. With improved calibration methodologies, reference-compensated measurement schemes, and further development of chronic implantation, more robust quantification and long-term monitoring will become feasible, which extends the applicability of FO-SPR sensing *in vivo*. This work therefore provides a proof-of-concept for plasmonic fiber-based biosensing in complex *in vivo* environments.

■ EXPERIMENTAL SECTION

Materials

Vancomycin hydrochloride, polyethylene glycol (PEG)-dithiol (MW: 3.4 kDa), lithium phenyl(2,4,6-trimethylbenzoyl) phosphinate (LAP), 1-dodecanthiol (DDT), and tris(2-carboxyethyl)phosphine hydrochloride (TCEP) were purchased from Sigma-Aldrich. UltraPure distilled water, 10× concentrated phosphate-buffered saline (PBS) pH 7.4 (RNase-free), magnesium chloride, calcium chloride, and sodium chloride were procured from Thermo Fisher Scientific. HPLC-grade ethanol was acquired from Carl Roth GmbH + Co. KG. Eight-arm PEG norbornene (10 kDa) was purchased from Creative PEGWorks. 1,4-Dithiothreitol (DTT) (99%) was acquired from Carl Roth GmbH. The vancomycin-binding P27 ssDNA split-aptamer sequences[41] with 5′ C6 S-S and 3′ C3 S-S thiol modifiers were synthesized by Integrated DNA Technologies for hydrogel conjugation to generate the aptagel, as described previously.[38] Vancomycin monitoring was performed in assay buffer (PBS with 2 mM $MgCl_2$ at pH 7.4), horse serum (Gibco, cat. no. 16050130), and human plasma (from teams TMI and PTA at BioMed X Institute GmbH).

FO-SPR Probe Fabrication

FO-SPR probes were constructed using multimode, step-indexed optical fibers (FT300UMT, Thorlabs Inc.) with a 300 μm-diameter pure silica core (refractive index 1.458, numerical aperture 0.39). The fibers were cut into 6.5 cm sections using a ruby-bladed fiber optic scriber to ensure flat end faces. A 3 mm region at one fiber end was designated as the sensing area. To fabricate FO-SPR probes, the protective coating was removed using a stripping tool (T16S31, Thorlabs Inc.), and the Technology Enhanced Clad Silica (TECS) cladding was dissolved in acetone. The flatness of fiber end faces was verified with a fiber inspection tool (FS201-SMA adaptor, Thorlabs Inc.). The exposed core of the fiber tips was sequentially cleaned with isopropanol and ethanol, followed by drying with a stream of nitrogen gas. Finally, the fiber tips were coated with a uniform 45 nm gold layer using a sputter coater (EM ACE600, Leica Microsystems, EMBL Imaging Centre).

https://doi.org/10.1021/acssensors.6c00681
ACS Sens. 2026, 11, 5858−5868

Deposition was performed on a rotating stage at a rate of 0.11 nm/s, following parameters adapted from Hasler et al.[29]

FO-SPR Sensor Setup

The optical fiber sensor setup consisted of a broadband white light source (HL-2000-LL, Ocean Insight, Orlando, Florida) and a high-resolution linear silicon array CCD spectrometer (FLAME-T-XR1-ES, Ocean Insight). Both were connected via SMA 905 connection outputs to a 1 × 2 (50:50) Y-multimode fiber optic coupler (300 μm core, Thorlabs Inc.). One arm of the coupler was connected to the light source, and the other to the FO-SPR probe through an SMA 905 multimode connector (340 μm bore, stainless-steel ferrule, Thorlabs Inc.) joined with an SMA-SMA mating sleeve to ensure optimal optical transmission. The sensing end of the fiber was secured in a strain-free bare fiber terminator (Newport, USA). Incident light in the visible range (wavelength of 400−1100 nm) was guided to the probe, and the reflected signal from the metal-dielectric interface was collected through the Y-coupler to the detector. Prior to measurements, the reflected light spectrum in air was normalized against the backlight reflection from the Y-coupler without the probe attached. Normalized reflectivity spectra R were processed using custom LabView software.[58] The plasmon resonant wavelength (λ_{SPR}) was tracked over time (t) to obtain sensor readout by centroid fitting the minimum of the spectra at a 20 nm window.

Aptagel FO-SPR Probe

The sensing matrix, aptagel, was prepared by embedding the vancomycin-binding split-aptamer pair into an eight-arm PEG-NB hydrogel crosslinked with dithiolated PEG and aptamer segments, as previously described.[38] The optimized formulation contained 3 mM aptamer with a macromer-to-crosslinker molar ratio of 4. The gold-coated FO-SPR probes were first incubated in 50 mM ethanolic DTT for 5 h and then in 50 mM ethanolic DDT for 5 min. They were then rinsed with ethanol and water and dried under nitrogen. Pregel solutions were pre-incubated at 37 °C for 2 h and then applied to fiber tips by submersion for 3 s and crosslinking under 365 nm UV light for 10 s. The coating step was repeated three times to ensure uniform gel coverage.

Scanning Electron Microscopy (SEM)

To verify gel coating on the fiber tips, aptagel-coated FO-SPR fibers were cut with a ruby blade to obtain clean cross sections. Three fibers were prepared, with cuts made ∼2 mm above the flat fiber end. Both bare and aptagel-coated probes were examined using a field-emission SEM (ZEISS Crossbeam 550, EMBL). Secondary electron and energy-selective backscatter modes were used to visualize probe architecture. Cross-sectional images were analyzed with ImageJ to assess coating morphology and structural integrity.

In Vitro Vancomycin Monitoring

FO-SPR probes were inserted to a 3 mm depth through a 1 mm opening into a vertical flow cell (∼24 μL volume) constructed using PDMS. Inlet and outlet tubing (Tygon, Ismatec, 0.25 mm ID) connected to a peristaltic pump (Ismatec) maintained a constant flow rate of 50 μL/min. The flow cell was mounted on a heater and enclosed in a custom Teflon block to maintain 37 °C. Prior to sensing, aptagel-coated probes were equilibrated in assay buffer under flow at 37 °C until fully swollen and a stable baseline λ_{SPR} was recorded for ≥15 min. Vancomycin-spiked solutions were then introduced to monitor analyte association, followed by vancomycin-free buffer for dissociation. Measurements were performed in assay buffer, 20% human plasma, and undiluted horse serum. Sensor limits of detection (LOD) were determined from dose−response curves by linear regression, with the LOD defined as the intercept concentration corresponding to 3× the standard deviation (σ) of the baseline. Sensorgrams were analyzed using Origin 2024 (v10.1).

Aptagel FO-SPR Probe Implantation

Male Wistar rats (320−360 g; Janvier, France) were used for *in vivo* FO-SPR implantation. Animals were group-housed under a 12 h light/dark cycle (lights on at 06:00) in temperature-controlled (21−22 °C) and humidity-controlled (55−65%) rooms with free access to food and water. All *in vivo* procedures were approved by Regierungspraesidium Tuebingen, Germany, and performed in an AAALAC (Association for Assessment and Accreditations of Laboratory Animal Care International)-accredited facility in accordance with the European Convention for Animal Care and Use of Laboratory Animals.[59] For implantation, rats were anesthetized with isoflurane and mounted in a stereotaxic frame (Kopf Model 1900). Anesthesia was maintained with 0.2−2% isoflurane throughout the experiment. After exposing the skull, a craniotomy was performed, and FO-SPR probes were inserted into the left cortex (stereotaxic coordinates: AP + 0.5, ML −3.0, DV −3.0 mm from bregma).[59]

In Vivo Vancomycin Monitoring

Approximately 2 h after probe implantation (equilibration), rats received vancomycin (75 or 150 mg/kg; i.v.; 2 mL/kg) or vehicle (0.9% NaCl; i.v.; 2 mL/kg) under continuous sensor recording. At the end of the experiments, animals were euthanized with sodium pentobarbital (100 mg/kg, i.p.). The time-dependent SPR wavelength shifts ($\Delta\lambda_{SPR}$) were baseline-corrected for drift and converted to vancomycin concentrations using calibration curves generated in undiluted horse serum. Calibration was based on log-linear fitting, where the slope and intercept parameters from the regression were applied to *in vivo* $\Delta\lambda_{SPR}$ values to reconstruct PK concentration−time profiles.

■ ASSOCIATED CONTENT

Supporting Information

The Supporting Information is available free of charge at https://pubs.acs.org/doi/10.1021/acssensors.6c00681.

Background information of split-aptamer and aptagel, dose-dependent response curve of the aptagel sensor for vancomycin detection in diluted human blood plasma, specificity analysis of the aptagel FO-SPR sensor against vancomycin, and full-time-range raw *in vivo* data (DOCX)

■ AUTHOR INFORMATION

Corresponding Author

Khulan Sergelen – *BioMed X Institute, Heidelberg 69120, Germany*; orcid.org/0000-0002-0546-3587; Email: sergelen@bmedx.com

Authors

Pragnya Satapathy – *BioMed X Institute, Heidelberg 69120, Germany*; Present Address: Manipal Institute of Applied Physics, Manipal Academy of Higher Education, Manipal, Karnataka 576104, India

Soohyun Park – *BioMed X Institute, Heidelberg 69120, Germany*; orcid.org/0000-0003-3261-7585

Anil Pal – *BioMed X Institute, Heidelberg 69120, Germany*; Present Address: Manipal Institute of Applied Physics, Manipal Academy of Higher Education, Manipal, Karnataka 576104, India

Catia Santa – *BioMed X Institute, Heidelberg 69120, Germany*

Eliza Koros – *N&MH-Neuroscience and Mental Health, Boehringer Ingelheim Pharma GmbH & Co. KG, Biberach an der Riß 88400, Germany*

https://doi.org/10.1021/acssensors.6c00681
ACS Sens. 2026, 11, 5858−5868

Judith Schweimer – *N&MH-Neuroscience and Mental Health, Boehringer Ingelheim Pharma GmbH & Co. KG, Biberach an der Riß 88400, Germany*; orcid.org/0000-0002-5968-3534
Roger Hasler – *LiST-Life Sciences Technology, Danube Private University, Neustadt 2700, Austria*; orcid.org/0000-0002-0883-3053
Jakub Dostalek – *LiST-Life Sciences Technology, Danube Private University, Neustadt 2700, Austria; FZU-Institute of Physics, Czech Academy of Sciences, Prague 180 00, Czech Republic*; orcid.org/0000-0002-0431-2170
Heather Clark – *School of Biological and Health Systems Engineering, Arizona State University, Tempe, Arizona 85281, United States*; orcid.org/0000-0002-2628-9194
Roberto Arban – *N&MH-Neuroscience and Mental Health, Boehringer Ingelheim Pharma GmbH & Co. KG, Biberach an der Riß 88400, Germany*
Bastian Hengerer – *N&MH-Neuroscience and Mental Health, Boehringer Ingelheim Pharma GmbH & Co. KG, Biberach an der Riß 88400, Germany*

Complete contact information is available at: https://pubs.acs.org/doi/10.1021/acssensors.6c00681

Author Contributions

[§]P.S. and S.P. contributed equally to this work.

Notes

K.S., S.P., P.S., and C.S. are listed as inventors on a patent (WO/2026/013312) describing a "Molecularly responsive hydrogel-based biosensor".

■ ACKNOWLEDGMENTS

We gratefully acknowledge our collaborators at Boehringer Ingelheim Pharma GmbH & Co. KG, Alica Maurer, and Andreas Genewsky for their technical support for *in vivo* measurements, Patrizia Voehringer and Carsten Wotjak and Hugh Marston for their guidance and facilitating access to infrastructure. We thank Alessio De Serafino for assistance in sensor preparation and Emre Kul for assistance in experimental procedure. We acknowledge the access and services provided by the Imaging Centre at the European Molecular Biology Laboratory (EMBL IC). Specifically, we are grateful for Robert Kirmse (Leicalabs@EMBL IC, Leica Microsystems GmbH) and Anna Steyer (EMBL IC) for their timely and dedicated support. R.H. acknowledges financial support by the Austrian Research Promotion Agency (FFG) within the COMET Project "PI-SENS" (Project No 915477) as well as by the Federal Provinces of Lower Austria and Tirol. J.D. is grateful for the support from the Czech Science Fund (GACR) project APLOMA (22-30456J) from the Operational Programme Johannes Amos Comenius financed by European Structural and Investment Funds and the Czech Ministry of Education, Youth and Sports (Project No. SENDISO -CZ.02.01.01/00/22_008/0004596). This work was supported by BioMed X Institute funding to K.S. from Boehringer Ingelheim Pharma GmbH & Co. KG.

■ REFERENCES

(1) Mir, M.; Palma-Florez, S.; Lagunas, A.; López-Martínez, M. J.; Samitier, J. Biosensors Integration in Blood–Brain Barrier-on-a-Chip: Emerging Platform for Monitoring Neurodegenerative Diseases. *ACS Sens.* **2022**, *7* (5), 1237–1247.
(2) Neumaier, F.; Zlatopolskiy, B. D.; Neumaier, B. Drug Penetration into the Central Nervous System: Pharmacokinetic Concepts and In Vitro Model Systems. *Pharmaceutics* **2021**, *13* (10), No. 1542.
(3) Scida, K.; Ornelas-Gatdula, E.; DePasquale, M.; Carr, G. V.; Arroyo-Currás, N. Therapeutic Drug Distribution across the Mouse Brain Is Heterogeneous as Revealed by In Vivo, Spatially Resolved Aptamer-Based Sensing. *ACS Pharmacol. Transl. Sci.* **2025**, *8* (2), 435–445.
(4) Blecka, L. J.; Jackson, G. J. Immunoassays in Therapeutic Drug Monitoring. *Clin. Lab. Med.* **1987**, *7* (2), 357–370.
(5) Clarke, W. Chapter 5 - Immunoassays for Therapeutic Drug Monitoring and Clinical Toxicology. In *Methods of Therapeutic Drug Monitoring Including Pharmacogenetics*; Hempel, G., Ed.; Handbook of Analytical Separations, Elsevier Science B. V., **2020**, *7*, 97–114.
(6) Cannon, D. J. Instrumentation and Techniques for Therapeutic Drug Monitoring. *Clin. Lab. Med.* **1987**, *7* (2), 325–334.
(7) Veringa, A.; Sturkenboom, M. G. G.; Dekkers, B. G. J.; Koster, R. A.; Roberts, J. A.; Peloquin, C. A.; Touw, D. J.; Alffenaar, J.-W. C. LC-MS/MS for Therapeutic Drug Monitoring of Anti-Infective Drugs. *TrAC Trends Anal. Chem.* **2016**, *84*, 34–40.
(8) Millington, D. S.; Kodo, N.; Norwood, D. L.; Roe, C. R. Tandem Mass Spectrometry: A New Method for Acylcarnitine Profiling with Potential for Neonatal Screening for Inborn Errors of Metabolism. *J. Inherit. Metab. Dis.* **1990**, *13* (3), 321–324.
(9) Gaspar, V. P.; Ibrahim, S.; Zahedi, R. P.; Borchers, C. H. Utility, Promise, and Limitations of Liquid Chromatography-Mass Spectrometry-Based Therapeutic Drug Monitoring in Precision Medicine. *J. Mass Spectrom.* **2021**, *56* (11), No. e4788.
(10) Vieira, P. A.; Shin, C. B.; Arroyo-Currás, N.; Ortega, G.; Li, W.; Keller, A. A.; Plaxco, K. W.; Kippin, T. E. Ultra-High-Precision, in-Vivo Pharmacokinetic Measurements Highlight the Need for and a Route Toward More Highly Personalized Medicine. *Front. Mol. Biosci.* **2019**, *6*, No. 69.
(11) Yang, J.; Gong, X.; Zheng, Y.; Duan, H.; Chen, S.; Wu, T.; Yi, C.; Jiang, L.; Haick, H. Microneedle-Based Integrated Pharmacokinetic and Pharmacodynamic Evaluation Platform for Personalized Medicine. *Nat. Commun.* **2025**, *16* (1), No. 6260.
(12) Yin, J.; He, X.; Wang, K.; Xu, F.; Shangguan, J.; He, D.; Shi, H. Label-Free and Turn-on Aptamer Strategy for Cancer Cells Detection Based on a DNA–Silver Nanocluster Fluorescence upon Recognition-Induced Hybridization. *Anal. Chem.* **2013**, *85* (24), 12011–12019.
(13) Yan, X.; Song, Y.; Zhu, C.; Song, J.; Du, D.; Su, X.; Lin, Y. Graphene Quantum Dot–MnO2 Nanosheet Based Optical Sensing Platform: A Sensitive Fluorescence "Turn Off–On" Nanosensor for Glutathione Detection and Intracellular Imaging. *ACS Appl. Mater. Interfaces* **2016**, *8* (34), 21990–21996.
(14) Williams, R. M.; Lee, C.; Galassi, T. V.; Harvey, J. D.; Leicher, R.; Sirenko, M.; Dorso, M. A.; Shah, J.; Olvera, N.; Dao, F.; Levine, D. A.; Heller, D. A. Noninvasive Ovarian Cancer Biomarker Detection via an Optical Nanosensor Implant. *Sci. Adv.* **2018**, *4* (4), No. eaaq1090.
(15) Guo, L.; Jackman, J. A.; Yang, H.-H.; Chen, P.; Cho, N.-J.; Kim, D.-H. Strategies for Enhancing the Sensitivity of Plasmonic Nanosensors. *Nano Today* **2015**, *10* (2), 213–239.
(16) Cho, H.; Yeh, E.-C.; Sinha, R.; Laurence, T. A.; Bearinger, J. P.; Lee, L. P. Single-Step Nanoplasmonic VEGF165 Aptasensor for Early Cancer Diagnosis. *ACS Nano* **2012**, *6* (9), 7607–7614.
(17) Armstrong, R. E.; Horáček, M.; Zijlstra, P. Plasmonic Assemblies for Real-Time Single-Molecule Biosensing. *Small* **2020**, *16* (52), No. 2003934.
(18) Rong, G.; Corrie, S. R.; Clark, H. A. In Vivo Biosensing: Progress and Perspectives. *ACS Sens.* **2017**, *2* (3), 327–338.
(19) Arroyo-Currás, N.; Somerson, J.; Vieira, P. A.; Ploense, K. L.; Kippin, T. E.; Plaxco, K. W. Real-Time Measurement of Small Molecules Directly in Awake, Ambulatory Animals. *Proc. Natl. Acad. Sci.* **2017**, *114* (4), 645–650.

(20) Shaver, A.; Mahlum, J. D.; Scida, K.; Johnston, M. L.; Aller Pellitero, M.; Wu, Y.; Carr, G. V.; Arroyo-Currás, N. Optimization of Vancomycin Aptamer Sequence Length Increases the Sensitivity of Electrochemical, Aptamer-Based Sensors In Vivo. *ACS Sens.* **2022**, *7* (12), 3895−3905.
(21) Li, H.; Dauphin-Ducharme, P.; Arroyo-Currás, N.; Tran, C. H.; Vieira, P. A.; Li, S.; Shin, C.; Somerson, J.; Kippin, T. E.; Plaxco, K. W. A Biomimetic Phosphatidylcholine-Terminated Monolayer Greatly Improves the In Vivo Performance of Electrochemical Aptamer-Based Sensors. *Angew. Chem., Int. Ed.* **2017**, *56* (26), 7492−7495.
(22) Booth, M. A.; Erdal, M. K.; Larson, M.; Birthisel, E.; Friedel, M.; Gonçales, V. R.; Alinezhad, A.; Morawski, F.; Li, J.; Hogan, N.; Teo, S.; Wordsworth, J.; Khanna, S.; Van Eps, J.; Boyd, S.; Dewhirst, L.; Gerson, J.; D'Souza, D.; Yin, W.; Padmanabhan, P. T.; Batchelor, R. H.; Farnkopf, A.; Hodges, A.; Chambers, G.; Braude, M.; Kippin, T. E.; Kirkpatrick, C. M. J.; Justin Gooding, J.; Pianko, S.; Stocker, S. L.; Plaxco, K. W. Pilot Phase Clinical Trial of a Wearable, Electrochemical Aptamer-Based Patch for Continuous Drug Concentration Measurement. *Nat. Biotechnol.* **2026**, 1−9.
(23) Bartnik, K.; Koba, M.; Śmietana, M. Advancements in Optical Fiber Sensors for in Vivo Applications − A Review of Sensors Tested on Living Organisms. *Measurement* **2024**, *224*, No. 113818.
(24) Esfahani Monfared, Y. Overview of Recent Advances in the Design of Plasmonic Fiber-Optic Biosensors. *Biosensors* **2020**, *10* (7), No. 77.
(25) Wen, Z.; Dong, Z.; Deng, Q.; Pang, C.; Kaminski, C. F.; Xu, X.; Yan, H.; Wang, L.; Liu, S.; Tang, J.; Chen, W.; Liu, X.; Yang, Q. Single Multimode Fibre for in Vivo Light-Field-Encoded Endoscopic Imaging. *Nat. Photonics* **2023**, *17* (8), 679−687.
(26) Zeni, L.; Perri, C.; Cennamo, N.; Arcadio, F.; D'Agostino, G.; Salmona, M.; Beeg, M.; Gobbi, M. A Portable Optical-Fibre-Based Surface Plasmon Resonance Biosensor for the Detection of Therapeutic Antibodies in Human Serum. *Sci. Rep.* **2020**, *10* (1), No. 11154.
(27) Loyez, M.; DeRosa, M. C.; Caucheteur, C.; Wattiez, R. Overview and Emerging Trends in Optical Fiber Aptasensing. *Biosens. Bioelectron.* **2022**, *196*, No. 113694.
(28) Gong, P.; Li, X.; Zhao, Q.; Zhou, X.; Zhang, Y.; Zhao, Y. Lab on a Single Fiber: A Three-Parameter Sensor Based on Triple-SPR for One-to-One Detection of DNA, PH and Temperature. *Sens. Actuators, B* **2024**, *401*, No. 134957.
(29) Hasler, R.; Reiner-Rozman, C.; Fossati, S.; Aspermair, P.; Dostalek, J.; Lee, S.; Ibáñez, M.; Bintinger, J.; Knoll, W. Field-Effect Transistor with a Plasmonic Fiber Optic Gate Electrode as a Multivariable Biosensor Device. *ACS Sens.* **2022**, *7* (2), 504−512.
(30) Lv, J.; Wang, J.; Yang, L.; Liu, W.; Fu, H.; Chu, P. K.; Liu, C. Recent Advances of Optical Fiber Biosensors Based on Surface Plasmon Resonance: Sensing Principles, Structures, and Prospects. *Sens. Diagn.* **2024**, *3* (9), 1369−1391.
(31) Dillen, A.; Mohrbacher, A.; Lammertyn, J. A Versatile One-Step Competitive Fiber Optic Surface Plasmon Resonance Bioassay Enabled by DNA Nanotechnology. *ACS Sens.* **2021**, *6* (10), 3677−3684.
(32) Ran, Y.; Xu, Z.; Chen, M.; Wang, W.; Wu, Y.; Cai, J.; Long, J.; Chen, Z.-S.; Zhang, D.; Guan, B.-O. Fiber-Optic Theranostics (FOT): Interstitial Fiber-Optic Needles for Cancer Sensing and Therapy. *Adv. Sci.* **2022**, *9* (15), No. 2200456.
(33) Hojjat Jodaylami, M.; Falardeau, D.; Malescot, A.; Rungta, R. L.; Kolta, A.; Masson, J.-F. Intracranial Surface-Enhanced Raman Scattering Endoscopy for In Vivo Protein Quantification under Physiological Stimulation. *ACS Sens.* **2025**, *10* (11), 9057−9067.
(34) Li, S.; Dai, J.; Zhu, M.; Arroyo-Currás, N.; Li, H.; Wang, Y.; Wang, Q.; Lou, X.; Kippin, T. E.; Wang, S.; Plaxco, K. W.; Li, H.; Xia, F. Implantable Hydrogel-Protective DNA Aptamer-Based Sensor Supports Accurate, Continuous Electrochemical Analysis of Drugs at Multiple Sites in Living Rats. *ACS Nano* **2023**, *17* (18), 18525−18538.
(35) Wareham-Mathiassen, S.; Jolly, P.; Radha Shanmugam, N.; Jagannath, B.; Prabhala, P.; Zhai, Y.; Ozkan, A.; Naziripour, A.; Singh, R.; Bengtsson, H.; Bjarnsholt, T.; Ingber, D. E. An Antimicrobial and Antifibrotic Coating for Implantable Biosensors. *Biosensors* **2025**, *15* (3), No. 171.
(36) Chen, Y.; Fu, K. X.; Cotton, R.; Ou, Z.; Kwak, J. W.; Chien, J.-C.; Kesler, V.; Nyein, H. Y. Y.; Eisenstein, M.; Tom Soh, H. A Biochemical Sensor with Continuous Extended Stability in Vivo. *Nat. Biomed. Eng.* **2025**, 1517−1530.
(37) Clark, V.; Prasad, A.; Yuan, Y.; Demek, E.; Guzman, F.; Garcia, L. A.; Lukeman, P. S.; Powell-Gray, B.; Rodríguez-López, J.; Arroyo-Currás, N. Extending the Operational Lifespan of Nucleic Acid-Based Electrochemical Sensors via Protection against Hydrogen Peroxide and Oligonucleotide Displacement. *ACS Sens.* **2025**, *10* (7), 4945−4953.
(38) Park, S.; Gerber, A.; Santa, C.; Aktug, G.; Hengerer, B.; Clark, H. A.; Jonas, U.; Dostalek, J.; Sergelen, K. Molecularly Responsive Aptamer-Functionalized Hydrogel for Continuous Plasmonic Biomonitoring. *J. Am. Chem. Soc.* **2025**, *147* (13), 11485−11500.
(39) Bello, V.; Vandezande, W.; Daems, D.; Lammertyn, J. Design and Implementation of a Dual-Region Self-Referencing Fiber-Optic Surface Plasmon Resonance Biosensor. *ACS Sens.* **2022**, *7* (11), 3360−3368.
(40) Wang, W.; Mai, Z.; Chen, Y.; Wang, J.; Li, L.; Su, Q.; Li, X.; Hong, X. A Label-Free Fiber Optic SPR Biosensor for Specific Detection of C-Reactive Protein. *Sci. Rep.* **2017**, *7* (1), No. 16904.
(41) Santa, C.; Park, S.; Gejt, A.; Clark, H. A.; Hengerer, B.; Sergelen, K. Real-Time Monitoring of Vancomycin Using a Split-Aptamer Surface Plasmon Resonance Biosensor. *Analyst* **2025**, *150* (1), 131−141.
(42) Aktug, G.; Asai, N.; Bozdogan, A.; Santa, C.; Sergelen, K.; Dostalek, J. Tethered Split-Aptamer Biosensor for Plasmon-Enhanced Fluorescence-Based Continuous Monitoring of Vancomycin. *ACS Sens.* **2026**, *11*, 1348−1357.
(43) Schwerdt, H. N.; Zhang, E.; Kim, M. J.; Yoshida, T.; Stanwicks, L.; Amemori, S.; Dagdeviren, H. E.; Langer, R.; Cima, M. J.; Graybiel, A. M. Cellular-Scale Probes Enable Stable Chronic Subsecond Monitoring of Dopamine Neurochemicals in a Rodent Model. *Commun. Biol.* **2018**, *1* (1), No. 144.
(44) Taylor, I. M.; Patel, N. A.; Freedman, N. C.; Castagnola, E.; Cui, X. T. Direct in Vivo Electrochemical Detection of Resting Dopamine Using Poly(3,4-Ethylenedioxythiophene)/Carbon Nanotube Functionalized Microelectrodes. *Anal. Chem.* **2019**, *91* (20), 12917−12927.
(45) Dwivedi, Y. S.; Sharma, A. K.; Gupta, B. D. Influence of Skew Rays on the Sensitivity and Signal-to-Noise Ratio of a Fiber-Optic Surface-Plasmon-Resonance Sensor: A Theoretical Study. *Appl. Opt.* **2007**, *46* (21), 4563−4569.
(46) Zhang, Q.; Wang, Y.; Mateescu, A.; Sergelen, K.; Kibrom, A.; Jonas, U.; Wei, T.; Dostalek, J. Biosensor Based on Hydrogel Optical Waveguide Spectroscopy for the Detection of 17β-Estradiol. *Talanta* **2013**, *104*, 149−154.
(47) Villuendas, F.; Pelayo, J. Optical Fibre Device for Chemical Seming Based on Surface Plasmon Excitridon. *Sens. Actuators, A* **1990**, *23* (1), 1142−1145.
(48) Nutiu, R.; Li, Y. Structure-Switching Signaling Aptamers. *J. Am. Chem. Soc.* **2003**, *125* (16), 4771−4778.
(49) Qi, X.; Yan, X.; Zhao, Y.; Li, L.; Wang, S. Highly Sensitive and Specific Detection of Small Molecules Using Advanced Aptasensors Based on Split Aptamers: A Review. *TrAC Trends Anal. Chem.* **2020**, *133*, No. 116069.
(50) Rybak, M. J.; Le, J.; Lodise, T. P.; Levine, D. P.; Bradley, J. S.; Liu, C.; Mueller, B. A.; Pai, M. P.; Wong-Beringer, A.; Rotschafer, J. C.; Rodvold, K. A.; Maples, H. D.; Lomaestro, B. M. Therapeutic Monitoring of Vancomycin for Serious Methicillin-Resistant Staphylococcus Aureus Infections: A Revised Consensus Guideline and Review by the American Society of Health-System Pharmacists, the Infectious Diseases Society of America, the Pediatric Infectious Diseases Society, and the Society of Infectious Diseases Pharmacists. *Am. J. Health Syst. Pharm.* **2020**, *77* (11), 835−864.
(51) Litwack, G. Chapter 21 - Blood and Lymphatic System. *Hum. Biochem.*, Academic Press: Boston, **2018**, 681−708.
(52) Mathew, J.; Sankar, P.; Varacallo, MA. Physiology, Blood Plasma **2025**. https://www.ncbi.nlm.nih.gov/books/NBK531504/.

https://doi.org/10.1021/acssensors.6c00681
ACS Sens. 2026, 11, 5858−5868

(53) Shrivastav, A. M.; Cvelbar, U.; Abdulhalim, I. A Comprehensive Review on Plasmonic-Based Biosensors Used in Viral Diagnostics. *Commun. Biol.* **2021**, *4* (1), No. 70.
(54) Gerson, J.; Erdal, M.; Dauphin-Ducharme, P.; Idili, A.; Hespanha, J.; Plaxco, K.; Kippin, T. A High-precision View of Intercompartmental Drug Transport via Simultaneous, Seconds-resolved, in Situ Measurements in the Vein and Brain. *Br. J. Pharmacol.* **2024**, *181*, 3869−3885.
(55) Yuan, Y.; Scida, K.; Carr, G. V.; Grohn, K.; Arroyo-Currás, N. Multicompartment Drug Monitoring Reveals Paired Brain−Liver Kinetics and Selective Central Nervous System Barrier Permeability in Rats. *ACS Sens.* **2026**, No. 3748.
(56) Luer, M. S.; Neill, K. K.; Gurley, B. J.; Lamb Shannon, M.; Killian, A. D.; Rodvold, K. A. Fluctuations in Vancomycin CNS Tissue Concentrations Following Intermittent and Continuous Infusions in the Rat. *Neurol. Res.* **2004**, *26* (3), 312−315.
(57) Dauphin-Ducharme, P.; Yang, K.; Arroyo-Currás, N.; Ploense, K. L.; Zhang, Y.; Gerson, J.; Kurnik, M.; Kippin, T. E.; Stojanovic, M. N.; Plaxco, K. W. Electrochemical Aptamer-Based Sensors for Improved Therapeutic Drug Monitoring and High-Precision, Feedback-Controlled Drug Delivery. *ACS Sens.* **2019**, *4* (10), 2832−2837.
(58) Kotlarek, D.; Vorobii, M.; Ogieglo, W.; Knoll, W.; Rodriguez-Emmenegger, C.; Dostálek, J. Compact Grating-Coupled Biosensor for the Analysis of Thrombin. *ACS Sens.* **2019**, *4* (8), 2109−2116.
(59) Büttner-Ennever, J. The Rat Brain in Stereotaxic Coordinates, 3rd Edn. By George Paxinos and Charles Watson. San Diego: Academic Press 1996. *J. Anat.* **2002**, *191* (2), 315−317.

https://doi.org/10.1021/acssensors.6c00681
ACS Sens. 2026, 11, 5858−5868